

Spin-orbital entanglement and frustration in pyrochlores $A_2\text{Mo}_2\text{O}_7$

Hiroshi Shinaoka,^{1,*} Yukitoshi Motome,² Takashi Miyake,¹ and Shoji Ishibashi¹

¹*Nanosystem Research Institute "RICS", National Institute of Advanced Industrial Science and Technology (AIST), Umezono, Tsukuba 305-8568, Japan*

²*Department of Applied Physics, University of Tokyo, Hongo, Bunkyo-ku, Tokyo 113-8656, Japan*
(Dated: May 6, 2013)

Electronic and magnetic properties of molybdenum pyrochlores $A_2\text{Mo}_2\text{O}_7$ are studied by the fully relativistic density-functional theory plus on-site repulsion (U) method, with focusing on the insulating material $\text{Y}_2\text{Mo}_2\text{O}_7$. As U increases, the ground state turns from a ferromagnetic metal into an antiferromagnetic insulator. In the insulating phase, the system exhibits peculiar magnetic degeneracy, which suggests strong anisotropy in the effective magnetic interactions. Analyzing a three-orbital Hubbard model, we show that the degeneracy is not solely in spin but in the spin-orbital entangled object formed under the cooperation of the trigonal distortion, Coulomb interactions, and spin-orbit interaction. The orbital frustration in the $4d^2$ electronic configuration plays an important role. The results give a new insight into the spin-glass behavior in the insulating materials.

PACS numbers: 71.15.Mb, 75.10.Hk, 75.10.Dg

Spin and orbital degrees of freedom of electrons play a crucial role in strongly correlated electron systems. The two degrees of freedom are entangled with each other via strong Coulomb interactions and the relativistic spin-orbit interaction (SOI) [1]. In general, the entanglement through the former mechanism is important in $3d$ transition metal compounds, while the latter is dominant in $5d$ systems. The spin-orbital entanglement is a source of fascinating and intricate properties, such as complicated spin-orbital orderings [2] and topologically nontrivial states [3]. Meanwhile, further intriguing situation is brought about by geometrical frustration of the lattice structure [4, 5]. Frustration suppresses a simple-minded ordering, and the residual spin and orbital fluctuations can be an origin of interesting phenomena, such as heavy-fermion behavior and exotic orders.

A family of pyrochlore oxides $A_2B_2\text{O}_7$ is a model system for studying the effects of spin-orbital entanglement and geometrical frustration [6]. In particular, compounds with $B=\text{Mn}$, Mo , Ir , and Os are interesting as they exhibit a metal-insulator transition (MIT) by changing temperature (T), pressure, and A -site cations. For instance, in $3d$ systems with $B=\text{Mn}$, the importance of Coulomb interactions has been argued for the mechanism of MIT and giant magnetoresistance [7, 8]. On the other hand, for $5d$ pyrochlores with $B=\text{Ir}$ and Os , recent first-principles studies revealed that SOI plays a dominant role in determining their peculiar electronic and magnetic properties [9, 10].

Mo pyrochlores $A_2\text{Mo}_2\text{O}_7$ are of particularly interest as Mo $4d$ electrons are subject to both strong Coulomb interactions and SOI. The system exhibits MIT by A -site substitution [11–13] as well as external pressure [14, 15]. The compounds with relatively large A -site ionic radii, e.g., Nd and Sm , show ferromagnetic (FM) metallic behavior at low T , while those with smaller ionic radii, such as Y , Dy , and Tb , are insulating and exhibit a spin-glass

(SG) transition instead of conventional long-range ordering [16–20]. A Hartree-Fock approach using a realistic band structure showed that Coulomb repulsions play a central role in the metal-insulator transition and the competition between magnetic interactions [21]. The role of orbital ordering in the competition was studied by extended double-exchange models [22–24]. The SG behavior was also studied by a Heisenberg spin model coupled with local lattice distortions [25, 26]. In the previous studies, however, unified understanding of MIT and peculiar SG insulating state has not been reached yet. In particular, SOI was not treated on an equal footing to Coulomb interactions, though it will be crucial in the spin-orbital entanglement in the $4d$ system.

In this Letter, we investigate the electronic and magnetic properties in $A_2\text{Mo}_2\text{O}_7$ by the fully relativistic local spin density approximation(LSDA)+ U method. We find that, by increasing the electron correlation, the system exhibits MIT from a FM metal to an antiferromagnetic (AFM) insulator. Remarkably, the insulating phase retains peculiar magnetic degeneracy, which is not explained by a simple Heisenberg antiferromagnetic model. Analyzing the origin of the degeneracy by a generalized spin model and a multi-orbital Hubbard model, we reveal the crucial role of spin-orbital entanglement due to cooperative effects between SOI, Coulomb interactions, and trigonal distortion of MoO_6 octahedra.

We perform density-functional calculations with our computational code, QMAS (Quantum Materials Simulator) [27], using the projector augmented-wave method [28] and the LSDA+ U method [29–34] with a planewave cutoff energy of 40 Ry. The relativistic effect including SOI is fully considered using two-component wave functions [33, 34]. The following calculations were done for a typical insulating material $\text{Y}_2\text{Mo}_2\text{O}_7$ using the experimental lattice structure: the lattice constant $a = 10.21 \text{ \AA}$ [35] and the so-called u parameter

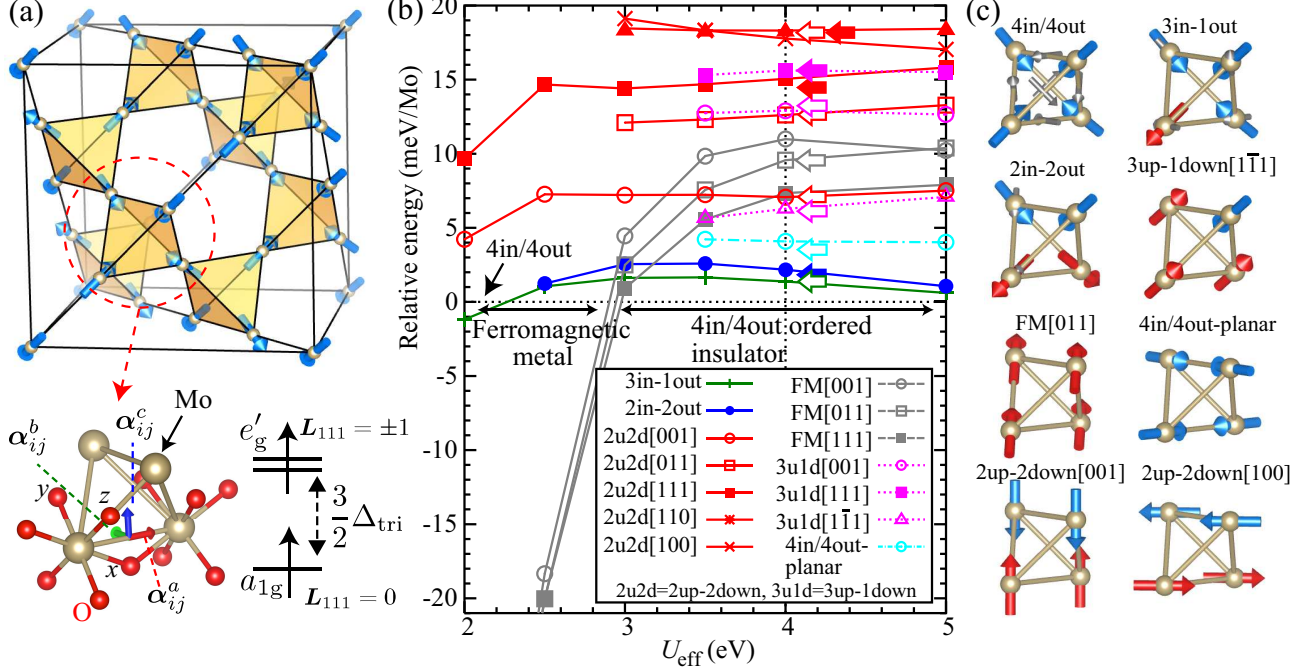


FIG. 1. (color online). (a) Cubic unit cell of a pyrochlore lattice, composed of Mo atoms in $A_2\text{Mo}_2\text{O}_7$. The arrows represent the Mo spin moments in the 4in/4out magnetic structure, which are along the local $[111]$ axes α_i^{111} . The circle denotes a primitive four-site unit cell, whose enlarged figure shows the local coordinates xyz and the vectors α_{ij}^k in the effective spin model in Eq. (1). The energy diagram shows the trigonal field splitting of t_{2g} orbitals. See the text for the details. (b) LSDA+ U results for U_{eff} dependences of energies for various $\mathbf{q} = 0$ magnetic states. The magnetic patterns are shown in (c). Energy is measured from that of the 4in/4out state. The arrows for the data at $U_{\text{eff}} = 4$ eV denote the energies calculated by the model (1). In the 4in/4out state in (c), small gray arrows denote the DM vectors α_{ij}^{DM} in the model (1).

$x(\text{O}_1) = 0.33821$ [36]. Every MoO_6 tetrahedron is compressed along the local $[111]$ axis (trigonal distortion) for $x(\text{O}_1) > 0.3125$ [see Fig. 1(a)]. We adopt a primitive unit cell with four Mo atoms. Experimentally, the magnetic and electronic properties vary systematically with the A-site ionic radius [11–13], which is regarded as the bandwidth control, namely, the control of electron correlation. We discuss such a systematic change by controlling the strength of electron correlation, $U_{\text{eff}} (\equiv U - J)$ [37], in the following.

Figure 1(b) shows the energies of various types of $\mathbf{q} = 0$ magnetic structures as functions of the Coulomb repulsion U_{eff} . Here we performed self-consistent calculations with constraints on the directions of Mo spin moments depending on each magnetic structure shown in Fig. 1(c). The system exhibits MIT at $U_{\text{eff}} \simeq 3$ eV from a FM metal to an AFM insulator while increasing U_{eff} ; the density of states (DOS) is shown in Fig. 2(a). Although MIT is consistent with the trend in the A-site substitution in $A_2\text{Mo}_2\text{O}_7$, the insulating state is experimentally SG instead of showing the AFM order. This discrepancy is discussed in detail below.

In the insulating region for $U_{\text{eff}} \gtrsim 3$ eV, the 4in/4out order is the most stable among the magnetic structures

considered [see Figs. 1(a) and 1(c)]. The Mo spin moment is $1.54 \mu_B$ at $U_{\text{eff}} = 4$ eV, indicating that a $S = 1$ spin is formed in the insulating phase by the Hund's coupling [Fig. 1(a)]. However, there are many other low-energy states, with their relative energies being almost independent of U_{eff} . In particular, the 3in-1out and 2in-2out states are almost degenerate with the 4in/4out ground state. This observation implies a substantial local $[111]$ easy-axis anisotropy, similarly to the case of $\text{Cd}_2\text{Os}_2\text{O}_7$ [10]. However, a simple $S = 1$ AFM spin model with the easy-axis anisotropy cannot account for the energy spectrum in Fig. 1(b). For example, FM[111]([011]) is always substantially lower in energy than 2up-2down[111]([011]), contrary to the expectation for the AFM model. This strongly suggests the existence of further intricate interactions.

In order to understand the results in Fig. 1(b), we consider a generalized Heisenberg model including all the symmetry-allowed pairwise interactions between nearest-neighbor (NN) spins [38, 39]. For simplicity, we restrict the consideration to classical spins. The Hamiltonian is

written in the form

$$\mathcal{H} = \sum_{\langle ij \rangle} \sum_{k=a,b,c} J_k (\mathbf{S}_i \cdot \boldsymbol{\alpha}_{ij}^k) (\mathbf{S}_j \cdot \boldsymbol{\alpha}_{ij}^k) + J_{\text{DM}} \sum_{\langle ij \rangle, i < j} \boldsymbol{\alpha}_{ij}^{\text{DM}} \cdot (\mathbf{S}_i \times \mathbf{S}_j) - D \sum_i (\mathbf{S}_i \cdot \boldsymbol{\alpha}_i^{111})^2 \quad (1)$$

where J_k are anisotropic NN exchange couplings between Mo spins \mathbf{S}_i and \mathbf{S}_j ; $\boldsymbol{\alpha}_{ij}^k$ are cubic axes on NN bonds [see Fig. 1(a)]. We take $|\mathbf{S}_i| = 1$. The second term denotes the Dzyaloshinsky-Moriya (DM) interaction between NN Mo atoms [40]. The DM vectors $\boldsymbol{\alpha}_{ij}^{\text{DM}}$ are shown in Fig. 1(c). The third term represents the single-ion anisotropy along the local $[111]$ axes $\boldsymbol{\alpha}_i^{111}$.

We determine the parameters in the model (1) so as to reproduce the energy levels in the insulating region in Fig. 1(b). We find that all the levels are well explained by taking $J_a > 0$, $J_b < 0$, $J_c < 0$, $J_{\text{DM}} < 0$, and $D > 0$. A typical result of the fitting is shown by the arrows in Fig. 1(b); the arrows indicate the energy levels calculated by the model (1) for $(J_a, J_b, J_c, J_{\text{DM}}, D) = (4.19, -2.94, -4.93, -4.21, 17.80)$ meV. The values are estimated by fitting the five independent low-lying states, the 3in-1out, 2up-2down[001], 2up-2down[011], 3up-1down[111], and FM[011], at $U_{\text{eff}} = 4$ eV. The results indicate that the effective spin model has surprisingly anisotropic interactions.

The degeneracy in Fig. 1(b) is understood by the competition between the AFM J_a and FM J_b , J_c , and negative J_{DM} . The former J_a favors 4in/4out rather than 2in-2out and 3in-1out, while the latter three do the opposite. The keen competition indicates that the system is in the competing regime between AFM and FM. Indeed, we confirmed that the ground state sensitively changes from 4in/4out to 2in-2out by a few % modification of the model parameters.

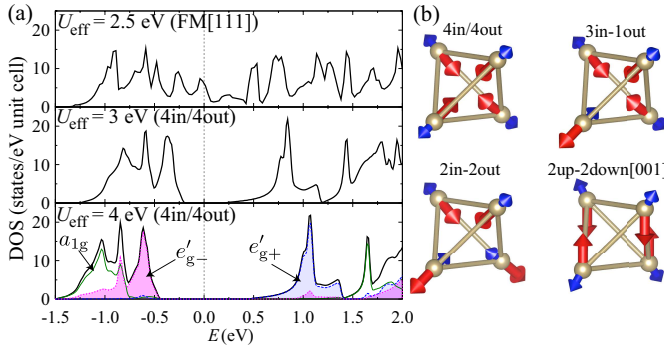


FIG. 2. (color online). (a) DOS calculated for the ground state at $U_{\text{eff}} = 2.5, 3$, and 4 eV. In the data at $U_{\text{eff}} = 4$ eV, the contributions from the a_{1g} and $e'_{g\pm}$ orbitals are also shown. (b) Spin \mathbf{S} (red bold arrows) and orbital moments \mathbf{L} (blue thin arrows) calculated at $U_{\text{eff}} = 4$ eV. The lengths of the arrows are proportional to the moment sizes, while those for \mathbf{L} are doubled for clarity.

The analysis clearly shows that not only spin but orbital degree of freedom plays a substantial role. To clarify the microscopic origin, we consider the orbital occupation by projecting DOS onto a_{1g} and $e'_{g\pm}$ orbital bases [41]: $|a_{1g}\rangle = (1, 1, 1)/\sqrt{3}$ and $|e'_{g\pm}\rangle = (e^{\pm 2\pi i/3}, 1, e^{\mp 2\pi i/3})/\sqrt{3}$, respectively, in the basis of d_{xy} , d_{yz} , and d_{zx} orbitals. The trigonal distortion splits the t_{2g} levels into a_{1g} and $e'_{g\pm}$, and each level has a quantized angular momentum along the local $[111]$ axis [see Fig. 1(a)]. As shown in Fig. 2(a), U_{eff} splits further the $e'_{g\pm}$ levels, and consequently, the a_{1g} and e'_{g-} orbitals are almost singly occupied, while the e'_{g+} orbital is mostly unoccupied in the insulating phase. Figure 2(b) shows the orbital moments \mathbf{L} as well as spin moments \mathbf{S} calculated for typical low-energy states at $U_{\text{eff}} = 4$ eV. It is obviously seen that \mathbf{L} is polarized almost along the local $[111]$ direction, being coupled with \mathbf{S} antiferromagnetically on each Mo atom. This strongly suggests that the orbital polarization plays a primary role in the anisotropic features in the effective spin model through SOI.

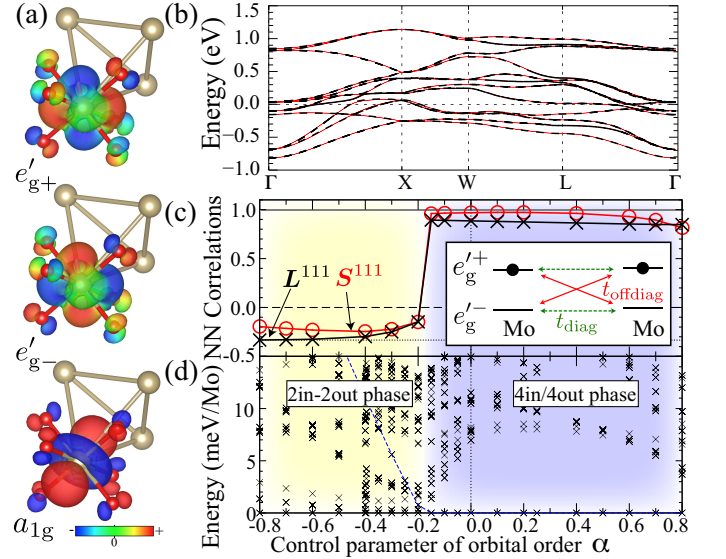


FIG. 3. (color online). (a) Density distribution of the MLWF localized at a Mo site obtained for $U_{\text{eff}}=0$. We take the $[001]$ axis as the quantization axis. The surface coloring represents the imaginary part ($e'_{g\pm}$) and real part (a_{1g}) of the wavefunctions of the majority spin component, respectively. (b) Non-magnetic band structure (solid curves). The broken curves represent the fit by MLWF. The energy is measured from the Fermi level. (c), (d) The NN correlation functions and the excitation spectrum of the three-orbital Hubbard model. The solid, broken, and dotted horizontal lines in (c) denote the NN correlations of \mathbf{L}^{111} for the 4in/4out, the 3in-1out, and the 2in-2out state in the classical limit, respectively. The inset shows the orbital off-diagonal (t_{offdiag}) and diagonal (t_{diag}) transfers between $e'_{g\pm}$ orbitals. The crosses connected by the broken line in (d) denote the 4in/4out energy.

Now, let us consider the intersite arrangement of the $e'_{g\pm}$ orbitals. The relative magnitude of the orbital di-

agonal and off-diagonal transfers (t_{diag} and t_{offdiag} , respectively) plays an important role in the orbital ordering [24]; under strong Coulomb interactions, t_{diag} (t_{offdiag}) favors an antiferro (ferro) orbital ordering to gain the second-order perturbation energy [see the inset of Fig. 3(c)]. Through the spin-orbital entanglement, the AFM 4in/4out state will be favored by ferro orbital ordering for $|t_{\text{offdiag}}| > |t_{\text{diag}}|$, while FM bonds in 3in-1out and 2in-2out by an antiferro orbital arrangement for $|t_{\text{offdiag}}| < |t_{\text{diag}}|$.

To explicitly demonstrate how the system is affected by the competition in the orbitals, we analyze a three-orbital Hubbard model for the t_{2g} orbitals by changing $|t_{\text{offdiag}}/t_{\text{diag}}|$. We use the values of $|t_{\text{offdiag}}| = 0.145$ and $|t_{\text{diag}}| = 0.102$ eV obtained by the maximally localized Wannier function (MLWF) analysis [42, 43] at $U_{\text{eff}} = 0$ as a reference [see Figs. 3(a) and 3(b)], and control the ratio by taking $t_{\text{offdiag}} \rightarrow (1+\alpha)t_{\text{offdiag}}$ and $t_{\text{diag}} \rightarrow (1-\alpha)t_{\text{diag}}$ with a control parameter α . We note that $|t_{\text{offdiag}}/t_{\text{diag}}|$ is ~ 1.4 for $0.33 \leq x(\text{O}_1) \leq 0.34$ [44], indicating that the following argument is robust for the series of $\text{A}_2\text{Mo}_2\text{O}_7$. The Hamiltonian includes the NN hopping term, SOI, trigonal splitting, and rotationally symmetric Coulomb interactions. We use the trigonal field $\Delta_{\text{tri}} = 0.25$ eV and SOI $\zeta = 0.085$ eV [45], which are obtained from the MLWF analysis. Setting the intraorbital Coulomb repulsion $U = 4$ eV and the Hund's coupling $J_{\text{H}} = 0.5$ eV, we performed perturbative calculations from the limit of strong Coulomb interactions up to the lowest order of SOI and transfer integrals.

Figures 3(c) and 3(d) show the NN correlation functions of \mathbf{L}^{111} and \mathbf{S}^{111} in the ground state and the calculated energy spectrum, respectively. Here, \mathbf{L}^{111} and \mathbf{S}^{111} are \mathbf{L} and \mathbf{S} projected on the local [111] axes, respectively. The results clearly show that the ground state turns from 2in-2out to 4in/4out by increasing α at $\alpha = \alpha_c \simeq -0.17$. For $\alpha > \alpha_c$, the 4in/4out ground state is singled out and largely separated from other excited states, as shown in Fig. 3(d). While decreasing α , however, the gap closes and there appears a large number of low-energy states near $\alpha \sim \alpha_c$. Although the MLWF estimate $\alpha = 0$ is in the 4in/4out region, it is close to the phase boundary. The result implies that this criticality gives the microscopic mechanism for the degeneracy and frustration in the spin-orbital entangled objects in Mo pyrochlores.

Our results provide a new insight into the emergence of the SG state. The frustration is not solely in spins but in the spin-orbital entangled degree of freedom. The frustrated spin-orbital entangled objects may be formed in the high- T PM phase, and freeze into a glass at low T due to inevitable randomness in real materials. Our results suggest that the competition between AFM 4in-4out and FM 2in-2out originating from orbital frustration plays a key role. Recently, the importance of local lattice distortions in the SG behaviors was pointed out

experimentally [46–50] and theoretically [25, 26]. The magnetoelastic coupling sensitively affects the degeneracy between the different spin-orbital configurations, as 2in-2out as well as 3in-1out can couple to local vibration modes of Mo tetrahedra [51, 52]. We therefore anticipate that these two configurations are energetically favored relative to AFM 4in/4out, resulting in further frustration with enhanced FM correlations.

To summarize, we found the peculiar magnetic degeneracy in the insulating phase of Mo pyrochlores. Through the analyses using the generalized effective spin model and three-orbital Hubbard model, we revealed the critical role of the spin-orbital entanglement and the degeneracy in the orbital sector in the peculiar magnetic properties.

We thank R. Kadono and H. Ohnishi for fruitful discussion. We also thank T. Kosugi for the use of his computational code. Numerical calculation was partly carried out at the Supercomputer Center, ISSP, Univ. of Tokyo. This work was supported by Grant-in-Aid for Scientific Research (No. 21340090, No. 22104010, No. 22540372, and No. 24340076), the Strategic Programs for Innovative Research (SPIRE), MEXT, and the Computational Materials Science Initiative (CMSI), Japan.

* Present address: Theoretische Physik, ETH Zurich, 8093 Zurich, Switzerland

- [1] K. I. Kugel and D. I. Khomskii, *Sov. Phys. Usp.* **25**, 231 (1982).
- [2] Y. Tokura and N. Nagaosa, *Science* **288**, 462 (2000), <http://www.sciencemag.org/content/288/5465/462.full.pdf>.
- [3] M. Z. Hasan and C. L. Kane, *Rev. Mod. Phys.* **82**, 3045 (2010).
- [4] H. Diep, *Frustrated Spin Systems* (World Scientific, Singapore, 2005).
- [5] F. M. C. Lacroix, P. Mendels, *Introduction to Frustrated Magnetism* (Springer-Verlag, Berlin Heidelberg, 2011).
- [6] J. S. Gardner, M. J. P. Gingras, and J. E. Greedan, *Rev. Mod. Phys.* **82**, 53 (2010).
- [7] M. A. Subramanian, B. H. Toby, A. P. Ramirez, W. J. Marshall, A. W. Sleight, and G. H. Kwei, *Science* **273**, 81 (1996), <http://www.sciencemag.org/content/273/5271/81.full.pdf>.
- [8] Y. Shimakawa, Y. Kubo, N. Hamada, J. D. Jorgensen, Z. Hu, S. Short, M. Nohara, and H. Takagi, *Phys. Rev. B* **59**, 1249 (1999).
- [9] X. Wan, A. M. Turner, A. Vishwanath, and S. Y. Savrasov, *Phys. Rev. B* **83**, 205101 (2011).
- [10] H. Shinaoka, T. Miyake, and S. Ishibashi, *Phys. Rev. Lett.* **108**, 247204 (2012).
- [11] J. Greedan, M. Sato, N. Ali, and W. R. Datars, *Journal of Solid State Chemistry* **68**, 300 (1987).
- [12] N. Ali, M. P. Hill, S. Labroo, and J. E. Greedan, *Journal of Solid State Chemistry* **83**, 178 (1989).
- [13] T. Katsufuji, H. Y. Hwang, and S.-W. Cheong, *Phys. Rev. Lett.* **84**, 1998 (2000).
- [14] S. Iguchi, N. Hanasaki, M. Kinuhara, N. Takeshita,

- C. Terakura, Y. Taguchi, H. Takagi, and Y. Tokura, Phys. Rev. Lett. **102**, 136407 (2009).
- [15] S. Iguchi, Y. Kumano, K. Ueda, S. Kumakura, and Y. Tokura, Phys. Rev. B **84**, 174416 (2011).
- [16] J. Greedan, M. Sato, X. Yan, and F. Razavi, Solid State Communications **59**, 895 (1986).
- [17] M. Sato and J. E. Greedan, Journal of Solid State Chemistry **67**, 248 (1987).
- [18] N. P. Raju, E. Gmelin, and R. K. Kremer, Phys. Rev. B **46**, 5405 (1992).
- [19] M. J. P. Gingras, C. V. Stager, B. D. Gaulin, N. P. Raju, and J. E. Greedan, J. Appl. Phys. **79**, 6170 (1996); **79**, 6170 (1996).
- [20] M. J. P. Gingras, C. V. Stager, N. P. Raju, B. D. Gaulin, and J. E. Greedan, Phys. Rev. Lett. **78**, 947 (1997).
- [21] I. V. Solovyev, Phys. Rev. B **67**, 174406 (2003).
- [22] Y. Motome and N. Furukawa, Phys. Rev. Lett. **104**, 106407 (2010).
- [23] Y. Motome and N. Furukawa, Phys. Rev. B **82**, 060407 (2010).
- [24] Y. Motome and N. Furukawa, Journal of Physics: Conference Series **320**, 012060 (2011).
- [25] H. Shinaoka, Y. Tomita, and Y. Motome, Phys. Rev. Lett. **107**, 047204 (2011).
- [26] H. Shinaoka, Y. Tomita, and Y. Motome, Journal of Physics: Conference Series **400**, 032087 (2012).
- [27] URL <http://qmas.jp/>.
- [28] P. E. Blöchl, Phys. Rev. B **50**, 17953 (1994).
- [29] D. M. Ceperley and B. J. Alder, Phys. Rev. Lett. **45**, 566 (1980).
- [30] J. P. Perdew and A. Zunger, Phys. Rev. B **23**, 5048 (1981).
- [31] I. V. Solovyev, P. H. Dederichs, and V. I. Anisimov, Phys. Rev. B **50**, 16861 (1994).
- [32] S. L. Dudarev, G. A. Botton, S. Y. Savrasov, C. J. Humphreys, and A. P. Sutton, Phys. Rev. B **57**, 1505 (1998).
- [33] T. Oda, A. Pasquarello, and R. Car, Phys. Rev. Lett. **80**, 3622 (1998).
- [34] T. Kosugi, T. Miyake, and S. Ishibashi, Journal of the Physical Society of Japan **80**, 074713 (2011).
- [35] J. S. Gardner, B. D. Gaulin, S.-H. Lee, C. Broholm, N. P. Raju, and J. E. Greedan, Phys. Rev. Lett. **83**, 211 (1999).
- [36] J. Reimers, J. Greedan, and M. Sato, Journal of Solid State Chemistry **72**, 390 (1988).
- [37] Refer to Refs. 31 and 32 for the definition of the LSDA+*U* energy functional.
- [38] G. Jackeli and G. Khaliullin, Phys. Rev. Lett. **102**, 017205 (2009).
- [39] B. J. Kim, H. Ohsumi, T. Komesu, S. Sakai, T. Morita, H. Takagi, and T. Arima, Science **323**, 1329 (2009), <http://www.sciencemag.org/content/323/5919/1329.full.pdf>.
- [40] M. Elhajal, B. Canals, R. Sunyer, and C. Lacroix, Phys. Rev. B **71**, 094420 (2005).
- [41] We constructed MLWF for the isolated t_{2g} manifold.
- [42] N. Marzari and D. Vanderbilt, Phys. Rev. B **56**, 12847 (1997).
- [43] I. Souza, N. Marzari, and D. Vanderbilt, Phys. Rev. B **65**, 035109 (2001).
- [44] Y. Moritomo, S. Xu, A. Machida, T. Katsufuji, E. Nishibori, M. Takata, M. Sakata, and S.-W. Cheong, Phys. Rev. B **63**, 144425 (2001).
- [45] ζ splits the t_{2g} level by $\frac{3}{2}\zeta$.
- [46] C. H. Booth, J. S. Gardner, G. H. Kwei, R. H. Heffner, F. Bridges, and M. A. Subramanian, Phys. Rev. B **62**, R755 (2000).
- [47] O. Ofer, A. Keren, J. S. Gardner, Y. Ren, and W. A. MacFarlane, Phys. Rev. B **82**, 092403 (2010).
- [48] A. Keren and J. S. Gardner, Phys. Rev. Lett. **87**, 177201 (2001).
- [49] E. Sagi, O. Ofer, A. Keren, and J. S. Gardner, Phys. Rev. Lett. **94**, 237202 (2005).
- [50] J. E. Greedan, D. Gout, A. D. Lozano-Gorrin, S. Derahkshan, T. Proffen, H.-J. Kim, E. Božin, and S. J. L. Billinge, Phys. Rev. B **79**, 014427 (2009).
- [51] O. Tchernyshyov, R. Moessner, and S. L. Sondhi, Phys. Rev. Lett. **88**, 067203 (2002).
- [52] O. Tchernyshyov, R. Moessner, and S. L. Sondhi, Phys. Rev. B **66**, 064403 (2002).